Waste Management 179 (2024) 163–174

Contents lists available at ScienceDirect

Waste Management

journal homepage: www.elsevier.com/locate/wasman

Research Paper

Waste-derived catalysts for tar cracking in hot syngas cleaning

Francesco Parrillo [a], Filomena Ardolino [a], Carmine Boccia [a,*], Vincenzo Arconati [a], Giovanna Ruoppolo [b], Umberto Arena [a]

[a] Department of Environmental, Biological, Pharmaceutical Sciences and Technologies – University of Campania "Luigi Vanvitelli", Via Vivaldi 43-81100, Caserta, Italy
[b] Institute of Sciences and Technologies for Sustainable Energy and Mobility, National Research Council-CNR. P.le Tecchio 1, 80125, Naples, Italy

ARTICLE INFO

Keywords:
Syngas cleaning
Tar cracking
Waste-derived catalysts
Waste gasification

ABSTRACT

Catalytic tar cracking is a promising technique for hot syngas cleaning unit in gasification plants because it can preserve tars chemical energy, so increasing the syngas heating value. The cost associated with catalyst preparation is a key issue, together with its deactivation induced by coke deposition. Iron is a cheap and frequently used catalyst, which can also be found in some industrial wastes. The study aims to assess the catalytic efficiency for tar cracking of two waste-derived materials (red mud and sewage sludge) having high content of iron. The catalysts were supported on spheres of γ-Al_2O_3, and their efficiency was compared to that of a pure iron catalyst. The role of support was investigated by testing pure red mud, with and without the support. A series of long-term tests using naphthalene as tar model compound were carried out under different values of process temperatures (750 °C-800 °C) and steam concentrations (0 %-7.5 %). The waste derived catalysts showed lower hydrogen yields compared to pure iron catalyst, due to their lower content of iron. On the other hand, the conversion efficiencies of all the tested catalysts resulted rather similar, since the Alkali and Alkaline-Earth Metallic species present on the surface of waste-derived catalyst help in preventing coke deposition. The iron oxidation state appears to play an important role, with reduced iron more active than its oxidised form in the tar cracking reactions. This indicates the importance of tuning steam concentration to keep constant the reduced state of iron while limiting coke deposition.

1. Introduction

Gasification is the thermochemical conversion of a carbonaceous solid or liquid material into a synthesis gas (syngas), composed of H_2, CO, and lower amounts of CH_4, together with different organic and inorganic impurities and particulates. These contaminants must be removed to allow the syngas use in different high-added value applications, such as high-efficiency electric energy generation, production of fuels, and synthesis of building block chemicals (Arena, 2013). Among the different contaminants, tars are the main compounds to deal with in the gasification processes. They are mixtures of high molecular weight hydrocarbons having high dew points, which lead to operating and environmental problems, such as clogging and corrosion of pipelines and auxiliary devices, catalyst damage, release of smelly gases. Tar removal technologies include physical and chemical techniques. Physical processes just transfer the tars from the gaseous phase to another phase, which then must be disposed of. Chemical processes allow to preserve tars chemical energy generally with the aid of a catalyst, by converting them into H_2 and CO, thus increasing the heating value of the syngas mixture (Anis & Zainal, 2011). The use of catalysts improves tar conversion and reduces the high temperatures required for its cracking (Li et al., 2015). However, different issues must be considered to enable an efficient tar cracking through catalytic processes at a Technology Readiness Level (TRL) suitable for commercial applications. The cost of catalytic materials is one of the main problems, together with limitations induced by deactivation phenomena of the active species.

Deactivation is a common phenomenon observed in tar cracking and reforming processes. Physical deactivation is mainly due to the

Abbreviations: AK, Activated carbon; AAEM, Alkali and Alkaline Earth Metal; ASTM, American Society for Testing and Materials; BET, Brunauer–Emmett–Teller; CHN, Carbon-Hydrogen-Nitrogen; DFT, Density Functional Theory; FBC, Fluidised Bed Combustion; GC–MS, Gas Chromatograph-Mass Spectrometer; GC-TCD, Gas Chromatograph-Thermal Conductivity Detector; ICP-MS, Inductively Coupled Plasma-Mass Spectrometry; RM, Red Mud; SEM-EDX, Scanning Electron Microscopy-Energy Dispersive X-Ray; SS, Sewage sludge; TRL, Technology Readiness Level; TPD, Temperature Programmed Desorption; TGA, Thermogravimetric Analysis; WG, Water-Gas; WGS, Water-Gas Shift; XRD, X-Ray Diffraction analysis.

* Corresponding author.
E-mail address: carmine.boccia@unicampania.it (C. Boccia).

https://doi.org/10.1016/j.wasman.2024.03.006
Received 13 December 2023; Received in revised form 7 February 2024; Accepted 5 March 2024
Available online 12 March 2024

deposition of coke, a by-product of tar cracking reactions, which covers active sites (Parrillo et al., 2023). Chemical deactivation is caused by the poisoning of active species due to impurities such as chlorine and sulphur (Yeo et al., 2019) and, at high temperature, to the sintering and then the agglomeration of low melting metals (Ochoa et al., 2018). This leads to phase changes resulting in surface area reduction (Duprez, 1992), loss of active metal by volatiles evaporation (Hunston et al., 2021; Yung et al., 2009) and diffusion on the support matrix (Bartholomew & Farrauto, 2010). While the use of a stable support can partially prevent chemical deactivation, the physical deactivation by coke remains one of the main limitations, leading to the loss of catalytic activity in a rather short time (Parrillo et al., 2023). Coke deposition can be limited by converting it into H_2 and CO through steam reforming and water–gas (WG) reactions. However, steam cannot completely avoid carbon deposition (Rostrup-Nielsen, 1984). It is therefore necessary to optimize the chemical physical characteristics of active catalyst to obtain higher tar conversion and minimising coke formation.

Carbonaceous catalysts such as Activated Carbon (AK) are commonly studied in recent years due to their high porosity and rather good content of Alkali and Alkaline-Earth Metallic (AAEM) species contained in the AK parent material (Fuentes-Cano et al., 2018; Di Gregorio et al., 2016). However, self-gasification phenomena under severe operating conditions and in presence of steam could limit their application at industrial scale. It is also complex to investigate the mechanism of deposition, since the coke and AK structure are often not easily distinguishable (Boccia et al., 2021). Non-carbonaceous catalysts, such as transition metals and their metal oxides, do not suffer problems of self-gasification and could help to better investigate the coke layer's nature under different operating conditions. This could also allow to partially prevent its formation or improve its conversion. Nickel-based catalysts show high tar removal efficiencies. However, they are expensive and sensible to deactivation due to coke formation and sintering of Ni^0. The reaction temperatures used in these processes (800 °C) are higher of the Tamman temperature of Ni, above which sintering occurs (Talebkeikhah et al., 2023). Moreover, small amounts of nitrogen, sulphur, and chlorine-containing compounds in the feed gas can poison the active sites, significantly reducing its performance, and further increasing operating costs due to frequent replacement (Gao et al., 2020). Iron-based catalysts are widely used in industrial Fischer-Tropsch synthesis (Dayton et al., 2019), and in the water–gas shift (WGS) processes (Jansen et al., 2015; Chianese et al., 2015). They have also shown good catalytic performances in tar cracking and reforming, both alone (Guan et al., 2016; Meng et al., 2019) and in combination with other active metals such as nickel (Bian et al., 2017; Koike et al., 2015). Iron could be found in different industrial by-products, which are low-cost materials that need to be safely disposed of. An example of waste materials rich in iron are the ashes from sewage sludge and red mud.

Sewage sludge is a liquid or semi-solid liquid generated from the wastewater treatment processes. The solid content ranges from 0.25 % to 12 % by weight (Djandja et al., 2022), and it is composed of water, organic matter, pathogens, but also inorganic components such as various types of salts (sulphates and phosphates), minerals (quartz, feldspars) and clays, among other substances. The annual production in the European Union of dry sewage sludge is between 6 and 9 million tonnes (Huygens et al., 2022), which is an excessive amount to be sent to landfill disposal. Thermochemical conversion such as incineration, gasification, and pyrolysis, have been recognised as the most promising alternatives to valorise the sewage sludge. They can reduce the amount of sewage sludge up to 70 % by mass, removing organic pollutants (Kang et al., 2023) and generating energy, fuels, and ashes with high concentrations of catalytic elements for tar cracking, especially iron (Ruoppolo et al., 2021). Red mud is a waste by-product of the Bayer process used to extract aluminium from bauxite ores, which is produced worldwide at a capacity of about 120 million tonnes each year (Silveira et al., 2021). Red mud is composed mainly of Fe_2O_3, Al_2O_3, SiO_2 and TiO_2 among other oxides (Kapelari et al., 2023; Nath et al., 2015; Gou et al., 2023), and its exact chemical composition depends on the place of origin. Due to its high basicity and potential leaching, its storage and disposal have critical environmental threats (Qi, 2021), and thus it is currently stored in dams. It is necessary to find industrial applications able to consume large volumes of this material and minimize its environmental impact. There are several studies on the application of red mud in the metallurgical and construction industry (Mahinroosta et al., 2020; Wang et al., 2021). Furthermore, some properties of red mud, such as its relatively high surface area, its inorganic composition with high iron content in the form of oxides such as FeO and Fe_2O_3, and the resistance to poisoning make it exploitable in chemical industries as an alternative to expensive metal oxide catalysts for different applications (Das and Mohanty, 2019; Shin and Kim, 2024; Zhang et al., 2024).

The conversion of waste residues into a potential resource such as catalyst for industrial processes is a very attractive option due to its high environmental and economic sustainability. However, their use in these applications is still at R&D stage, and more studies are needed to fully understand the true potentialities and limitations. Despite sewage sludge ashes and red mud have already been studied as catalysts in other fields, at the best of the author's knowledge only a few studies have been carried out on the use of these materials as catalysts for high-temperature tar cracking (Ruoppolo et al., 2021; Zhang et al., 2022; Wang et al., 2022a; Cheng et al., 2020). Ruoppolo et al. (2021) showed that sewage sludge ashes were more active on heavy hydrocarbons rather than light hydrocarbons as primary catalyst for gasification of wood with air. Zhang et al. (2022) tested a sewage sludge char conditioned with quicklime to reform the volatiles produced by sewage sludge pyrolysis at 750 °C. The conditioning improved the volatile reforming, and the sewage sludge char achieved 84.1 % conversion of mono-aromatic and 100 % conversion of oxygenated compounds. Wang et al. (2022a) tested a red mud catalyst supported on char. The obtained tar conversion efficiency was improved by the carbonaceous support which promotes Fe reduction and the dispersion of the active phase. Cheng et al. (2020) obtained similar results by using a combination of red mud and char in the cracking of naphthalene, under different atmosphere (CH_4, CO, CO_2, H_2O, H_2). These studies highlighted the positive effect of red mud and sewage sludge utilisation in catalytic applications. However, most of them used the catalysts in combination with various carbonaceous supports. The use of this type of material is tricky when dealing with syngas and steam, as the support itself is consumed by the reacting atmosphere, leading to a loss of material in longer duration tests (Boccia et al., 2021).

This study used naphthalene as a tar model compound and measured the removal efficiency obtained by using sewage sludge ashes and red mud, supported on alumina. The performances have been compared with those of a pure Fe-catalyst by means of a series of long-term tests, under different values of process temperatures (750 °C-800 °C) and steam concentrations (0 %-7.5 %). The role of the support has been also considered by testing pure red mud with and without the support. The study aims to assess the possibility of using new, cheap, and efficient catalysts for tar cracking compared to commercial catalysts, and to increase the knowledge about the effect of operating conditions on the catalyst performance.

2. Materials and methods

2.1. Tar model compound and catalysts

Naphthalene ($C_{10}H_8$) was used as tar model compound since it is recognised as one of the main and more stable hydrocarbons in a tar mixture obtained from waste and biomass gasification processes (Boccia et al., 2021; Parrillo et al., 2023). Table A.1 in Annex A reports the features of its solid crystals (as provided by Sigma Aldrich), which have been used during the tests.

The tested catalysts are industrial wastes produced in huge quantities: one is a red mud (RM), which is a residue of the Bayer process for

Table 1
Physical properties and inorganic composition of the fresh catalysts and their parent materials.

Physical properties						
	γ-Al_2O_3*	RM	SS**	RM/γ-Al_2O_3	SS/γ-Al_2O_3	Fe/γ-Al_2O_3***
Surface Area (m^2/g)	150–170	94.6	n.a.	156	146	147
Pore Volume (cm^3/g)	>0.45	0.20	n.a.	0.45	0.41	0.47
ICP MS analysis (mg/kg)**						
Li	–	6.0	–	0.3	–	–
Na	–	42,160	268	1294	331	–
K	–	680	1404	550.9	1423	–
Al	–	1960	4931	32,490	–	
Mg	–	997.5	2210	–	296	–
Ca	–	2662	10,320	–	4014	–
Zn	–	5.7	303	12.2	185	
Ti	–	21,630	–	507	–	–
V	–	377.3	–	28	–	–
Cr	–	394.8	–	13.0	–	–
Mn	15	283.0	122	11.6	29	–
Fe	217	124,300	14,170	3600	10,470	30,000
Co	–	24.1	–	0.1		–
Ni	–	42.6	41	–	12	–
Cu	118	8.4	171	–	249	–

*Supplied by Sasol Germany GmbH©; ** As received; ***Data from Parrillo et al., 2023.

the extraction of aluminium from bauxite; the other one (SS) derives from ashes obtained by a municipal sewage sludge (Fig. A.1 in the Annex A). Both have high concentrations of iron, a metal with known catalytic potential due to its tendency to donate or accept electrons. The efficiencies of these waste-derived catalysts were compared to those of a Fe-catalyst supported by γ-alumina (Fe/γ-Al_2O_3), used in many industrial processes and utilised in a previous experimental campaign (Parrillo et al., 2023). Fe/γ-Al_2O_3 was prepared with an iron content of 3 wt% by dissolving the corresponding amount of iron nitrate nonahydrate $Fe(NO_3)_3{\cdot}9H_2O$ (98+%, Sigma-Aldrich) in aqueous solution and adding a suitable amount of alumina support. The material was then dried at 120 °C for 12 h and calcined with air at 850 °C. The support allows to avoid loss of active metals by means of strong bounds formed between them. Alumina is one of the most used catalytic supports for tar reforming reactions due to its good mechanical strength, chemical/physical stability, great resistance to sintering, and high melting point (Prins, 2020; Ochoa et al., 2020). It was available as commercial γ-Al_2O_3 spheres produced by Sasol Germany GmbH©, having a diameter of 1 mm, a high specific surface of 150–170 m^2/g, a pore volume higher than 0.45 cm^3/g (Miccio et al., 2016), and a good resistance to high temperatures (He et al., 2018).

The first waste-derived catalyst, red mud, was used without (RM) and with support (RM/γ-Al_2O_3) to investigate the role of gamma-alumina on the catalytic performances. The supported red mud was prepared by using the same procedure adopted for the Fe/γ-Al_2O_3. An amount of RM corresponding to a load of active phase of about 5 wt% in the catalyst was suspended in deionised water and stirred by using a magnetic stirring. The γ-Al_2O_3 support was added, and the slurry was dried at 120 °C for 12 h in a rotavapor up to the complete vaporisation of water. This step was followed by calcination with air at 850 °C, to promote the chemical bonds between the active phase and support.

The unsupported red mud was instead first compressed to 5 bar and then crushed and sieved to obtain granules with a size range between 0.8 and 1.2 mm, similar to the diameter of the γ-Al_2O_3 spheres, to avoid any external diffusion limitation (Parrillo et al., 2020). The sewage sludge-derived catalyst (SS/γ-Al_2O_3) was prepared in a different way, since the procedure adopted for RM/γ-Al_2O_3 and Fe/γ-Al_2O_3 cannot be applied because SS ashes do not stick to the support surface. A fluidised bed combustor (FBC), with bed material made of γ-Al_2O_3 spheres, was fed with the dry sewage sludge, obtaining its complete burn-out. The sludges were treated for 220 min at 850 °C at a fluidization velocity of 1 m/s, and an air excess of 47 %. The discharged SS ashes appeared well adhered to the γ-Al_2O_3 particles and ready to be used as tar cracking catalyst. Fig. A.1 in the Annex schematically shows the catalysts used and the related preparation methods.

2.2. Apparatus and procedures for fresh and spent catalysts characterisation

Fresh and spent catalysts were characterised by different ways to acquire data and information that can support the interpretation of the experimental results. Fresh catalysts were analysed by means of i) ICP-MS, Inductively Coupled Plasma equipped with Mass Spectrometry, by using an Agilent 7500 CE instrument, to obtain their inorganic composition (Table 1); ii) TPD, Temperature Programmed Desorption, analysis, by using a Micromeritics TPD/TPR 2900 analyser, to estimate their acidity strength. Both fresh and spent catalysts were also characterised by means of i) BET, Brunauer–Emmett–Teller method, by N_2 adsorption at 77 K and the density functional theory (DFT) and Monte-Carlo simulation method (DFT Kernel), by using a Quantachrome Autosorb 1-C analyser, to determine the specific surface area, pore volume and pore size distribution (Tables 1 and 2); ii) TGA, Thermogravimetric Analysis, by using a TGA 701 LECO, to provide a reliable estimation of the mass variation of the whole bed of catalysts, before and after each test; iii) XRD, X-Ray Diffraction analysis, by using a Rigaku Miniflex 600, to investigate the surface composition, the degree of crystallinity of the pure catalyst and the active sites dispersion on the support. The peak recognition was carried out with the support of the QUALX2.0 software (Altomare et al., 2015), while the crystallite size was measured by Scherrer Equation (Behrens and Schlögl, 2012); iv) SEM-EDX, Scanning Electron Microscopy with Energy Dispersive X-Ray Analysis, by using a Field Electron and Ion Inspect™ S50 SEM, to study the catalyst surface by providing detailed high-resolution images of the catalysts surface. Finally, ultimate analyses were carried out by using a CHN 2000 LECO elemental analyser, according to the ASTM D5373, to obtain information about the coke layer that covers their surface: these deposits have been recognised as the main issue for tar cracking and reforming processes (Boccia et al., 2021).

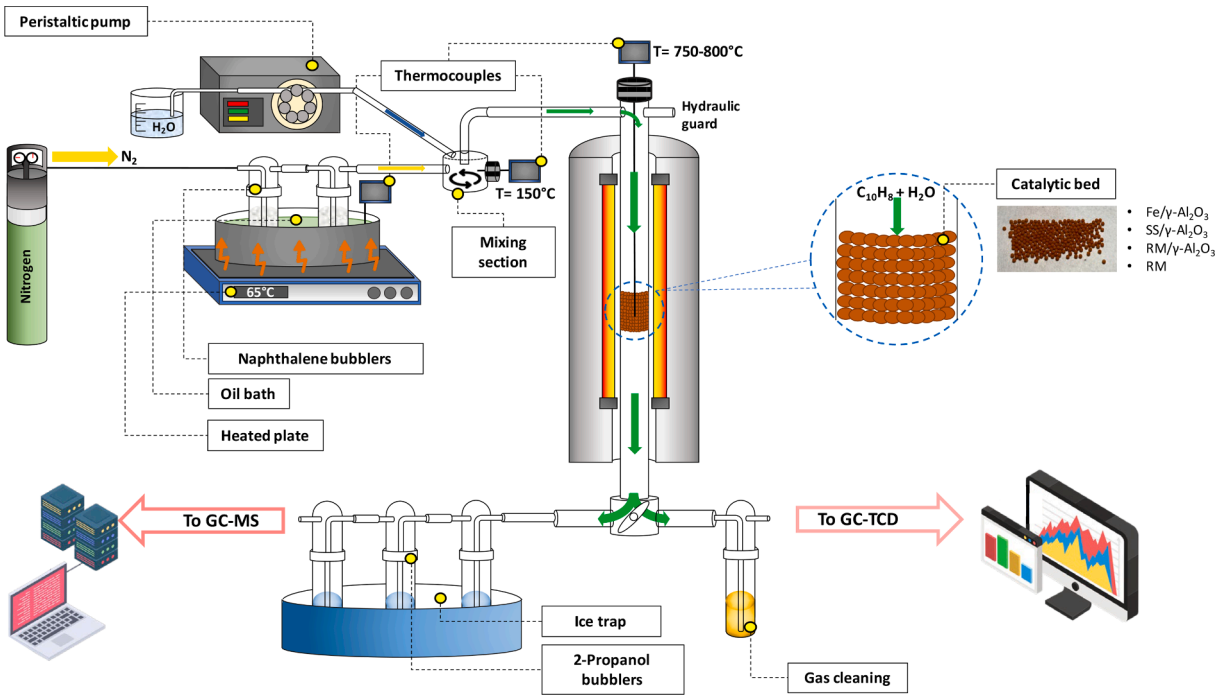

Fig. 1. Schematic representation of the experimental apparatus.

2.3. Apparatus and procedures for experimental tests

The tests were carried out in a bench-scale tubular quartz reactor having an internal diameter of 14 mm and a total height of 600 mm (Fig. 1). A detailed description of the apparatus is reported elsewhere (Boccia et al., 2021). Nitrogen was used as inert carrier gas and fed into two bubblers, each containing 20 g of solid crystal of naphthalene. The bubblers were kept at 65 °C in an oil bath to allow the vaporization of naphthalene. Steam was fed by a peristaltic pump (Ismatec Regloo Digital 2-Channel©) and vaporised in a 15 cm long pipe kept at 150 °C. The generated steam was mixed with nitrogen and naphthalene in a mixing section before entering the reactor. All the lines of the feeding and exit sections were heated at 150 °C to avoid gas condensation. The produced gas was cleaned to remove residual naphthalene and water before its entrance in a gas chromatograph equipped with a thermal conductivity detector (GC-TCD, 3000a Micro GC), able to measure, every five minutes, the content of H_2, CO, CH_4, N_2, CO_2, and low molecular-weight hydrocarbons. The produced gas was then directed into a sampling section, made by three bubblers containing 2-propanol at 0 °C, by switching a three-way valve. The collected residual naphthalene was analysed by a gas chromatograph coupled with a mass spectrometer, GC–MS Agilent HP6890/HP5975.

The catalysts were tested in a N_2 atmosphere, by using a naphthalene concentration of 22.5 mg/L_N, without and with an addition of steam, and temperatures of 750 °C and 800 °C. The selected tar concentration, as well as the temperature and steam concentration, are typical values that can be found at the exit of a biomass/waste fluidized bed gasifier (Arena, 2013). The peristaltic pump was calibrated before each test to ensure a fixed concentration of 7.5 % of steam. This concentration was selected based on the previous study of Boccia et al. (2021), which investigated the effect of different steam concentration in the catalytic cracking of tars. A bed of 2.6 g of each supported catalyst was used to obtain a bed height of 3 cm, which gave a residence time of 0.11 s. The bed amount was increased to 3.6 g for the tests with pure RM, to keep gas residence time constant. When steam was added, the N_2 flowrate was adjusted according to the operating conditions selected to ensure the same total flowrate and concentrations. After the system reached the steady state, the nitrogen was sent to the bubblers and then to the reactor. The first naphthalene sample was collected 5 min after the start to assess the initial conversion efficiency of the catalytic bed. The successive samples were collected every 30 min for the first two hours of testing, and then every hour until the end of the tests, to assess the deactivation over time. The reactor was purged with N_2 and cooled down to room temperature after each test.

3. Results and discussion

3.1. Characterisation of the fresh catalysts

Physical properties and inorganic composition of the fresh catalysts and their parent materials are reported in Table 1. All the supported catalysts show specific surface areas of approximately 150–170 m^2/g, which is like that of pure γ-Al_2O_3, highlighting the positive contribution of this support. The unsupported RM, which was only compressed, shows a smaller specific surface of about 95 m^2/g. The iron content of the catalysts is different due to its concentration in the parent material and preparation method. RM shows the highest concentration of iron, ten time larger than that of pure SS. The waste-derived supported catalysts have an iron concentration lower than that of Fe/γ-Al_2O_3. All elements, including AEEM, are well distributed on the surface, as indirectly confirmed by the value of specific surface area that is rather close to that of pure γ-Al_2O_3.

The microscopic structure and physical features of the catalysts surface were analysed by SEM-EDX. Fig. B.1 in Annex B reports four SEM images together with a specific iron mapping related to each of them. Although these images refer to small areas of a highly magnified sample, they can provide useful information (Marsh & Rodriguez-Reinoso, 2006). The distribution of active material on the support appears homogenous, with the formation of clusters that occurred during the catalyst's preparation. The waste-derived supported catalysts, RM/γ-Al_2O_3 and SS/γ-Al_2O_3, present many nanoparticle clusters with an irregular morphology, as can be seen in Figs. B.1-B and B.1-C. These uneven clusters were produced during the preparation procedure and are made of nanoparticles of different compounds (metal oxides, silicon dioxide, and others). This could suggest an uneven distribution of active sites. The XRD analyses reported in Fig. 2 show however that spectra related

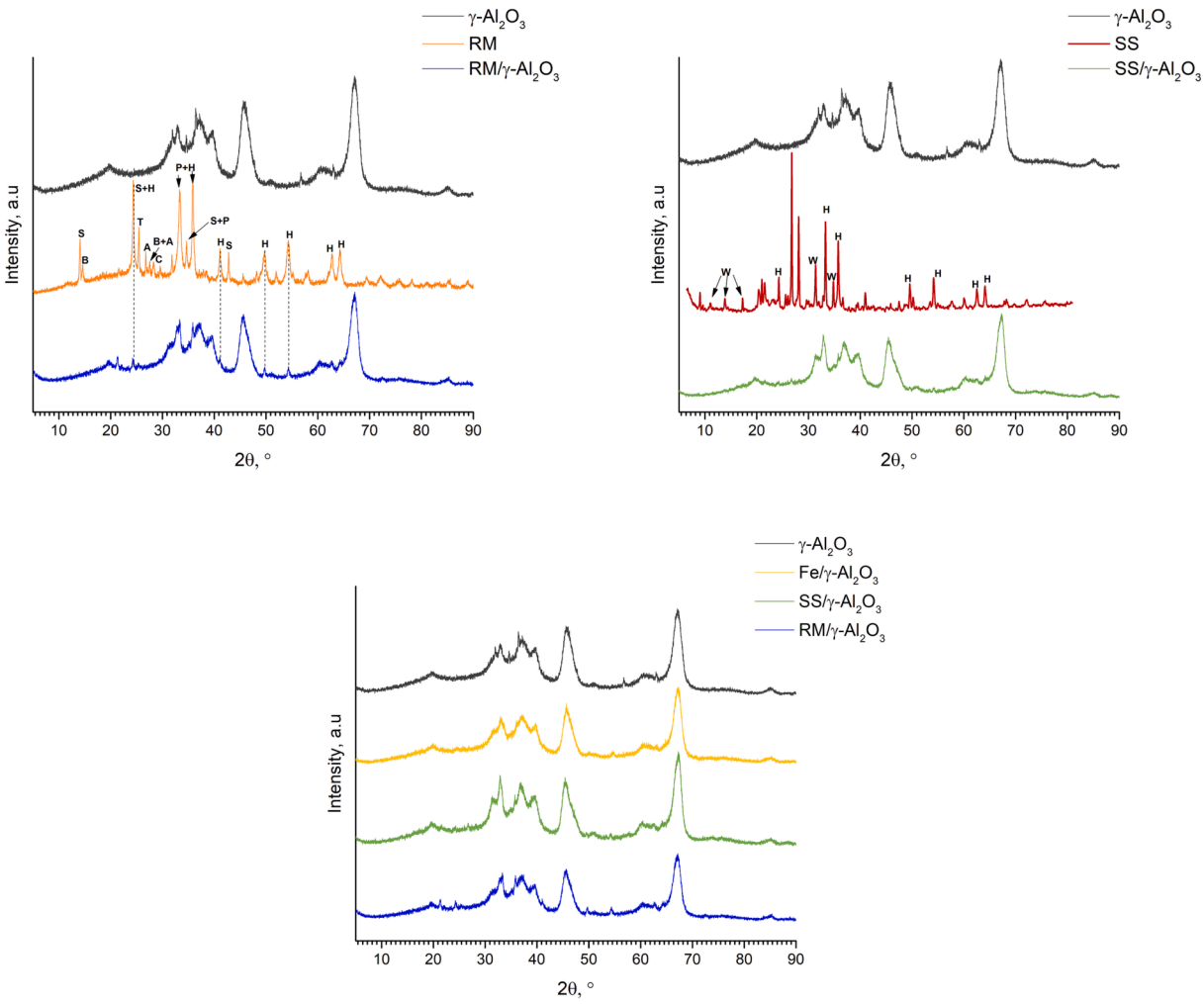

Fig. 2. XRD spectra of the fresh catalysts. Top-left: spectra for the γ-Al_2O_3 support, RM supported catalyst, and pure RM. Top-right: spectra for the γ-Al_2O_3 support, SS supported catalyst, and pure SS. Bottom: Spectra for the support and all the supported catalysts. Legenda: H, hematite; S, sodalite; B, boehmite; T, titania; A, aragonite; C, calcite; P, perovskite; W, whitlockite.

to pure γ-Al_2O_3, which predominate over those of active species, appear almost completely superimposable to those of RM/γ-Al_2O_3 and SS/γ-Al_2O_3. This indicates a homogenous distribution of the iron on the support surface, without any visible effect of the mentioned clusters. XRD spectra of pure RM and pure SS can be used to identify the content of main oxides since they are not affected by the γ-Al_2O_3 signal.

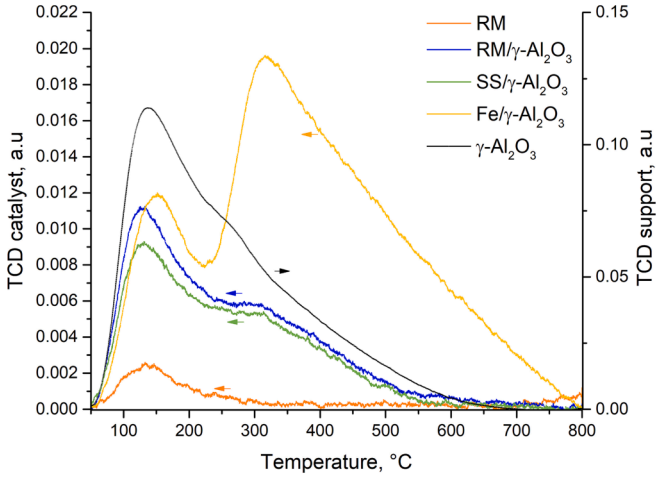

Fig. 3. TPD-NH_3 analyses of the different fresh catalysts and pure γ-Al_2O_3.

The RM spectrum (Fig. 2, top-left, orange line) shows peaks corresponding to aragonite ($CaCO_3$), hematite (Fe_2O_3), sodalite ($Na8(Al_6Si_6O_{24})Cl_2$), perovskite ($CaTiO_3$), boehmite (γ-AlO(OH)), calcite ($CaCO_3$), and titania (TiO_2). The dominant phases are hematite and sodalite, having an average crystallite size of 11.4 nm and 32.3 nm respectively, which was also detected in the RM/γ-Al_2O_3 catalyst. The XRD spectrum of SS (Fig. 2, top right, red line) shows the signal of whitlockite ($Ca_9(MgFe)(PO_4)_6PO_3OH$) and, in particular, of hematite (Fe_2O_3): this suggests that iron is largely present under its most oxidised form.

The acidic strength of the catalysts was assessed by a TPD analysis, which allows the quantification of acid sites on a catalytic surface by desorption of an alkaline probe molecule (Alreshaidan et al., 2022). The acidity plays a crucial role in various hydrocarbon catalytic reactions, including cracking, isomerisation, and polymerisation (Bartholomew & Farrauto, 2010). The acidity is also the main cause of coke deposition on the catalyst surface, due to the cleavage of C-C and C-H bonds (Jenness et al., 2014; Umansky et al., 1990). The TPD analyses of fresh catalysts are reported in Fig. 3.

The peaks on the obtained curves indicate the presence of acid sites with different strengths (Mosallanejad et al., 2018): the peaks at lower temperatures (150 °C–200 °C) could be associated to weak acidic sites, while those at higher temperatures (300 °C–400 °C) to medium acidic sites. All the supported catalysts exhibit both the acidic sites, while

unsupported RM shows a limited amount of only weak acidic sites: hence, the acidity is mainly a characteristic of the γ-Al_2O_3 support (Busca, 2019). The alkali compounds contained in RM and SS cause a decrease of acidic site concentration, as indicated by the amount of desorbed ammonia measured during the analyses (Zhang et al., 2020): pure γ-Al_2O_3 shows an amount of 4.69 mmol/g compared to those of 0.61 mmol/g and 0.52 mmol/g related to RM/γ-Al_2O_3 and SS/γ-Al_2O_3, respectively. The absence of alkali compounds on the surface of Fe/γ-Al_2O_3 causes a lower decrease of acidic sites, with an amount of desorbed ammonia of 1.67 mmol/g. The higher acidity of Fe/γ-Al_2O_3 implies a greater ability to break the tar molecules but, on the other hand, a greater tendency to accumulate coke on its surface, as reported by Feng et al. (2016).

3.2. Tar cracking tests

The experimental tests were carried out under the following operating conditions: naphthalene concentration = 22.5 mg/L_N; reactor temperature = 750 °C or 800 °C; carrier gas volumetric flow rate = 0.49 L_N/min or 0.47 L_N/min, to keep constant the gas residence time (0.11 s); and steam concentration = 0 % or 7.5 %. The tests aimed at evaluating the tar cracking efficiencies for each catalyst, comparing the related performances, and investigating the effect of reactor temperature and steam addition, at a fixed residence time.

3.2.1. Time evolution of gas composition

Fig. 4 reports the H_2 production for each catalyst under the different operating conditions tested. In the experiments without steam (Fig. 4 A and 4C), the trends appear not affected by temperature. RM, RM/γ-Al_2O_3 and SS/γ-Al_2O_3 show a low H_2 concentration in the first 25 min, which subsequently increases, being almost constant in the remaining time. The initial trends are not comparable to those obtained with Fe/γ-Al_2O_3 and may be attributed to the oxidation state of iron. The reduced Fe^0 has a greater activity in the cleavage of C-C and C-H bonds compared to that of Fe oxides because it allows a better overlap of atomic orbitals of the involved species (Wang et al., 2022a). Such feature is attributed to the absence of oxygen atoms in the lattice structure, which affects the intermolecular interactions due to steric hindrance (Chi et al., 2018). The waste-derived catalysts contain iron in oxidized form that could be reduced by hydrogen produced in the early stages, improving their performance. Viceversa, Fe/γ-Al_2O_3 is not fully oxidised and therefore already active in the first few minutes (Miccio et al., 2016). RM shows the lowest hydrogen trend but also a lower deactivation tendency. This could be related to its higher iron content and, above all, the presence on its surface of other inorganic elements that can hinder the accumulation of coke on the surface.

In the experiments with steam (Fig. 4B and 4D), the trends are clearly affected by temperature, since WG and WGS reactions are triggered at 800 °C. The waste-derived catalysts show lower H_2 yields than those generated by Fe/γ-Al_2O_3, which are approximately two times larger due to the higher iron content. H_2 yields appear rather constant for all catalysts up to six hours of testing (although the already mentioned activation phenomenon is visible in the first few minutes). Finally, the efficiency of the RM catalysts appears not favoured by steam concentration at 750 °C, as it is shown by Fig. B.2 in ANNEX B, since at this temperature the reforming reactions are not activated and, at the same time, steam increases the iron oxidation, reducing its catalytic activity (Cheng et al., 2020).

The measured time evolution of gas composition with steam allows comparing the concentration of the other produced gases (Fig. 5). Tests carried out with the two RM catalysts (Figures from 5A to 5D) show significant generation of CO_2 in the initial phase, which are likely related to the decomposition of carbonates such as aragonite and calcite, at both temperatures. This effect is more pronounced with pure RM, because of the higher content of these elements. SS-derived catalyst (Fig. 5E-5F) does not show this phenomenon since calcite and aragonite are not present in the parent material (as highlighted by Fig. 2). After the initial phase, CO_2 trends are stable for all the catalysts throughout the entire test duration. The CO behaviour is different since its production by WG reaction is strongly limited at 750 °C, and just increases at 800 °C, when reforming reactions are promoted (Daza & Kuhn, 2016; Kharaji et al., 2013).

3.2.2. Naphthalene conversion efficiency

Naphthalene was sampled at different time during each test to assess its conversion efficiency with the different catalysts (Fig. 6). The catalysts show rather similar conversion efficiencies, particularly under presence of steam. This appears not in agreement with the low yields of

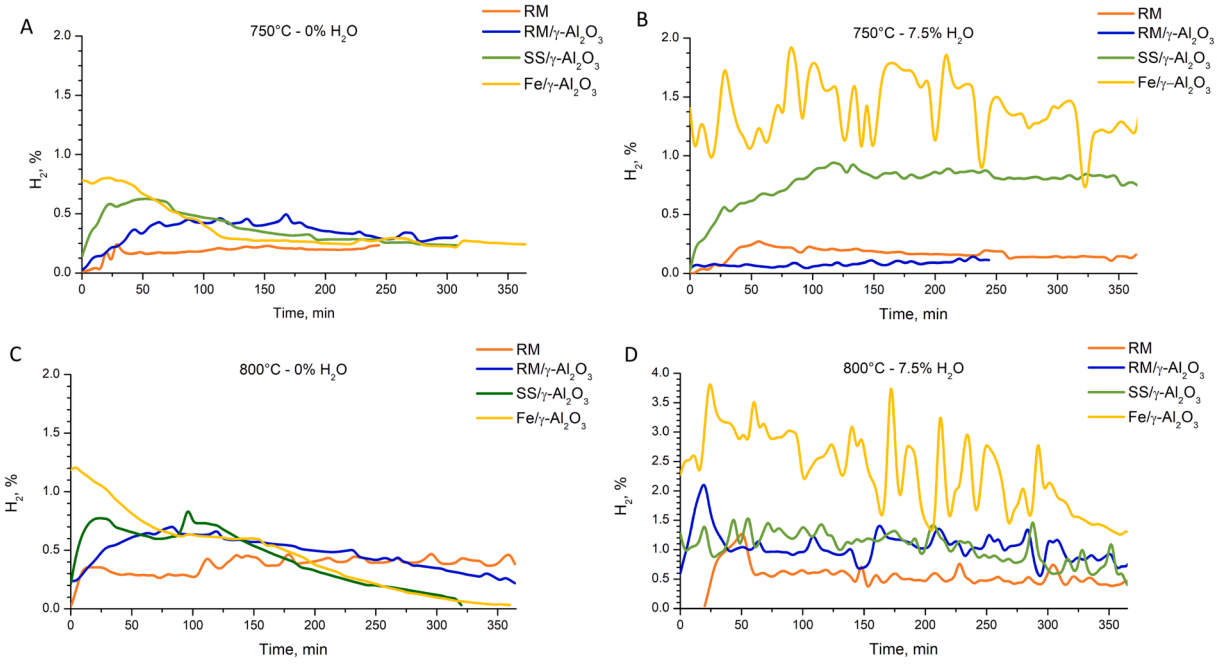

Fig. 4. Time evolution of H_2 under the different operating conditions tested.

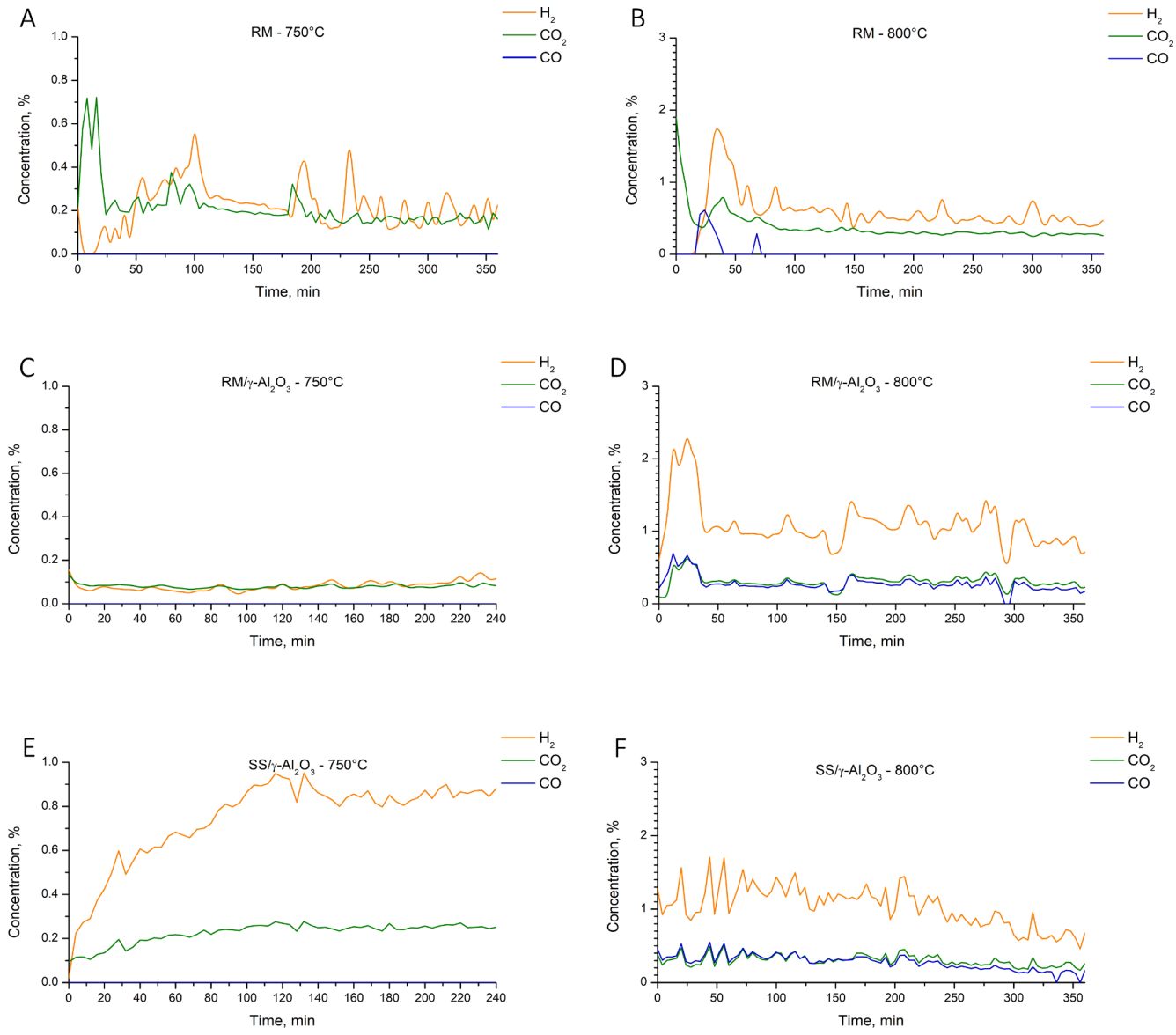

Fig. 5. Time evolution of the main gases produced in the tests with waste-derived catalysts under presence of steam.

hydrogen measured with waste-derived catalysts in the tests with steam (Fig. 4). A possible explanation could be the oxidation of part of the generated hydrogen to reduce the iron oxides present on the surface of the waste-derived catalysts. Fig. 6 also suggests that RM/γ-Al_2O_3, despite its lower concentrations of Fe and AAEMs (Table 1), has slightly higher conversion efficiencies compared to those of RM: this could confirm the positive role of the support, which in turn is related to a larger specific surface area and a better dispersion (and, likely, anchoring) of the active sites.

Reactor temperature has a positive effect on naphthalene conversion for all tested catalysts, in tests with and without steam, due to the endothermic nature of the reactions involved. Finally, deactivation phenomena after six hours were observed only with Fe/γ-Al_2O_3, at 800 °C and without steam: this is likely due to the absence of AAEM elements, which could favour coke deposition without any possibility of its conversion, as confirmed by the decrease of H_2 production (Fig. 4C). Fig. 6 also suggests that the main effect of steam appears to be that of promoting reforming reactions, and thus limiting coke deposition and allowing a longer activity time of the tested catalysts. Its expected contribution to an increase of naphthalene conversion efficiency, as already observed in tests with activated carbon catalysts (Boccia et al., 2021), appears rather limited. A possible explanation is that without steam, the more active Fe^0 is longer present on the catalyst surface, mainly due to hydrogen action. When steam is present, it competes with reducing gases by partially oxidising iron, so inhibiting its complete reduction, which leads to a decrease in the amount of naphthalene cracked, and to conversion efficiencies rather close to those obtained without steam. This effect of steam on the iron oxidation state can be directly observed (Fig. B3 in ANNEX B) by analysing the XRD spectra related to fresh and spent RM catalysts, after tests at 800 °C, with and without steam. The spectrum of the fresh catalyst indicates a predominant presence of hematite, which is the most oxidised form of iron; that of the spent catalyst after a test without steam, shows instead the predominance of reduced iron; finally, the spectrum of spent catalyst after a test with steam, highlights the predominance of magnetite, which is a form of intermediate oxidation of iron.

3.2.3. *Mass variation and catalyst surface characterisation*

Fig. 7 reports the mass variation of the catalysts at the end of the tests, carried out at 800 °C, without and with steam. Data are reported as time-specific unit, to compare tests having different duration (Ravenni et al., 2020). A positive mass variation indicates coke deposition on the

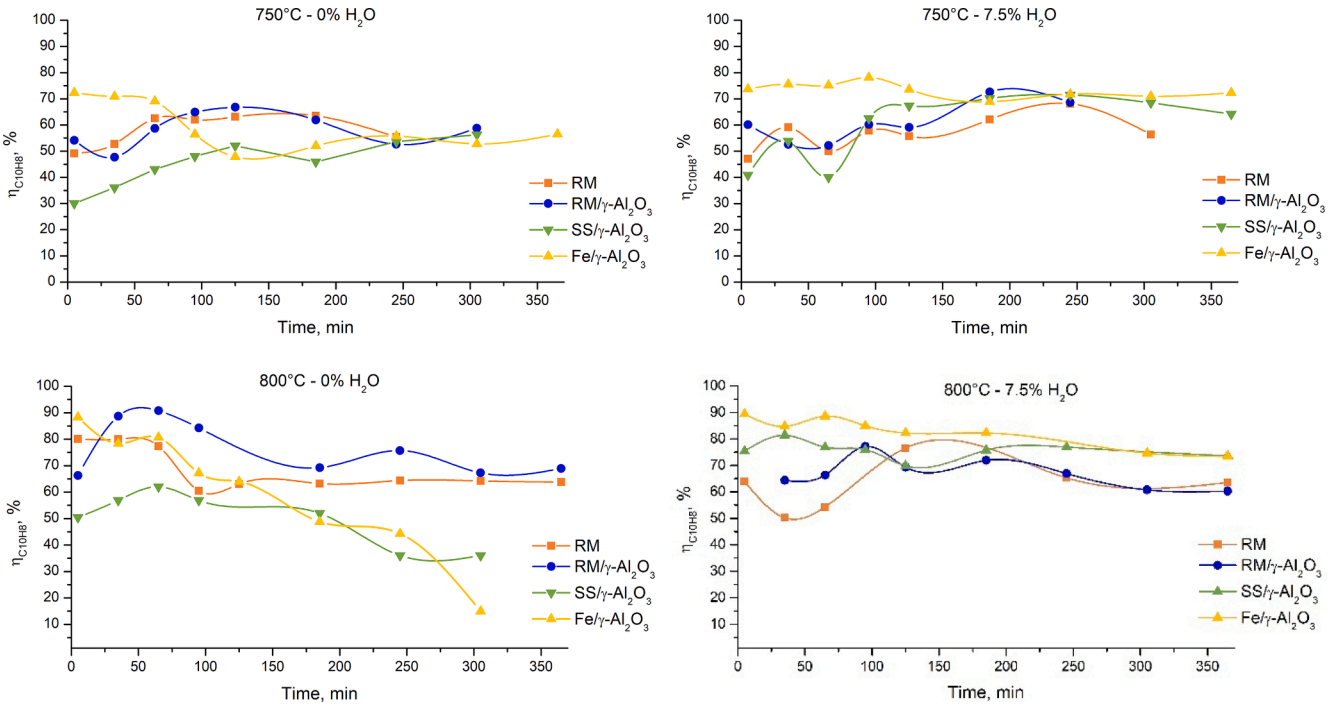

Fig. 6. Naphthalene conversion efficiencies under the different operating conditions tested.

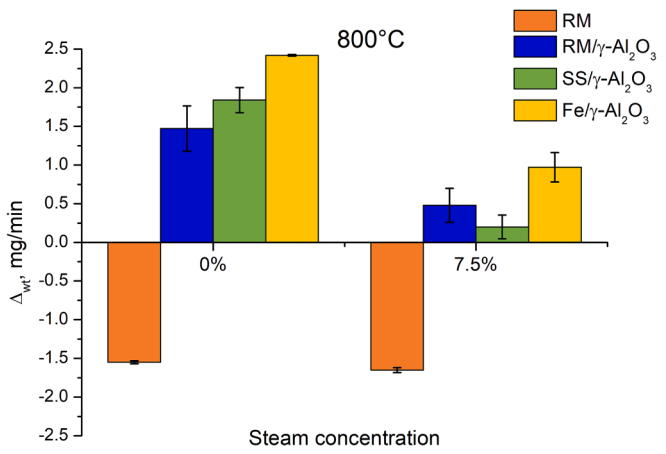

Fig. 7. Mass time variation of the catalysts at the different operating condition tested.

catalyst surface, due to naphthalene cracking (Parrillo et al., 2023); a negative variation indicates a degradation of the catalyst structure (Boccia et al., 2021). The highest mass variations were obtained without steam, due to the absence of any reforming agent, able to operate coke removal. Tests with steam were instead characterised by reduced mass variation for all the catalysts, being coke converted through WG and steam reforming reactions. SS/γ-Al_2O_3 and RM/γ-Al_2O_3 show a lower mass variation than that of Fe/γ-Al_2O_3, due to the combination of a slightly lower catalytic activity and the presence of AAEM elements on their surface which hinder the coke build-up (Feng et al., 2016). AAEMs have the potential to suppress carbon formation (Ashok et al., 2020), thus enhancing the quality of the gaseous products. The negative mass variations observed in the tests with unsupported RM is explained by its partial consumption: this makes challenging, or likely impossible, to assess the extent of coke deposition. With pure RM, the surface consumption due to the absence of support, causes a loss of about 1.5 mg/min of material: it is expected to lose all the material in tests longer than about 40 h. On the other hand, and until the complete loss of catalytic mass, this same consumption could improve the conversion efficiency by removing coke from the surface, so exposing new active elements.

A deeper investigation on the nature of coke layer required an analysis of spent catalysts obtained in all the tests. Fig. 8 reports the curves obtained by TGA with air, together with data of total mass loss (Δ_{wt}), measured by TGA, and carbon content, measured by CHN analyses. All fresh catalysts show only an initial weight loss around 100 °C, due to the evaporation of adsorbed water (RM/γ-Al_2O_3 and SS/γ-Al_2O_3 about 5 %, Fe/γ-Al_2O_3 about 2.5 %). Only spent catalysts also show another weight loss, starting after 400 °C, which further supports the presence of a coke layer. The TGA of RM/γ-Al_2O_3 and SS/γ-Al_2O_3 show different weight losses in the absence of steam. These variations, 13.9 % for SS/γ-Al_2O_3 (with a C content of 18 %) and 27.4 % for RM/γ-Al_2O_3 (with a C content of 22 %) are mainly attributed to carbon deposition. The lower variation measured for SS/γ-Al_2O_3 is attributed to the presence of higher amounts of active elements other than Fe, such as Ca and K, that hinder coke deposition (Table 1). Furthermore, the temperature at which coke starts to decompose is about the same for the different operating conditions tested (around 400 °C), suggesting the formation of a coke with a similar structure (Ochoa et al., 2020). Fe/γ-Al_2O_3 shows two different temperature of mass losses (400 °C, without steam, and 550 °C, with steam), suggesting different structures of coke, which could deposit on different parts of the surface, as further investigated by SEM observations reported in the following. TGA of pure RM show a completely different trend compared to the supported catalysts. Fresh sample shows a constant weight loss during the analysis (8 %), due to water evaporation at the initial stage, and dehydroxylation of bohemite and decomposition of carbonates at higher temperatures (Brostow & Datashvili, 2008; Madadkhani et al., 2021). Spent RM does not show a mass loss but instead a mass gain, of 1 % and 0.1 %, without and with steam, respectively, which can be attributed to the oxidation of magnetite into hematite by air. TGA of the sample from tests without steam shows another mass gain of 3.4 % in the temperature range 400 °C–450 °C, due to the oxidation of Fe^0 (Wang et al., 2022b; Lysenko et al., 2014). The presence of Fe^0 and magnetite is confirmed by the XRD analysis of the spent RM catalysts (Fig. B3 of ANNEX B), without and with steam, respectively. Finally, a coke layer should be present also on

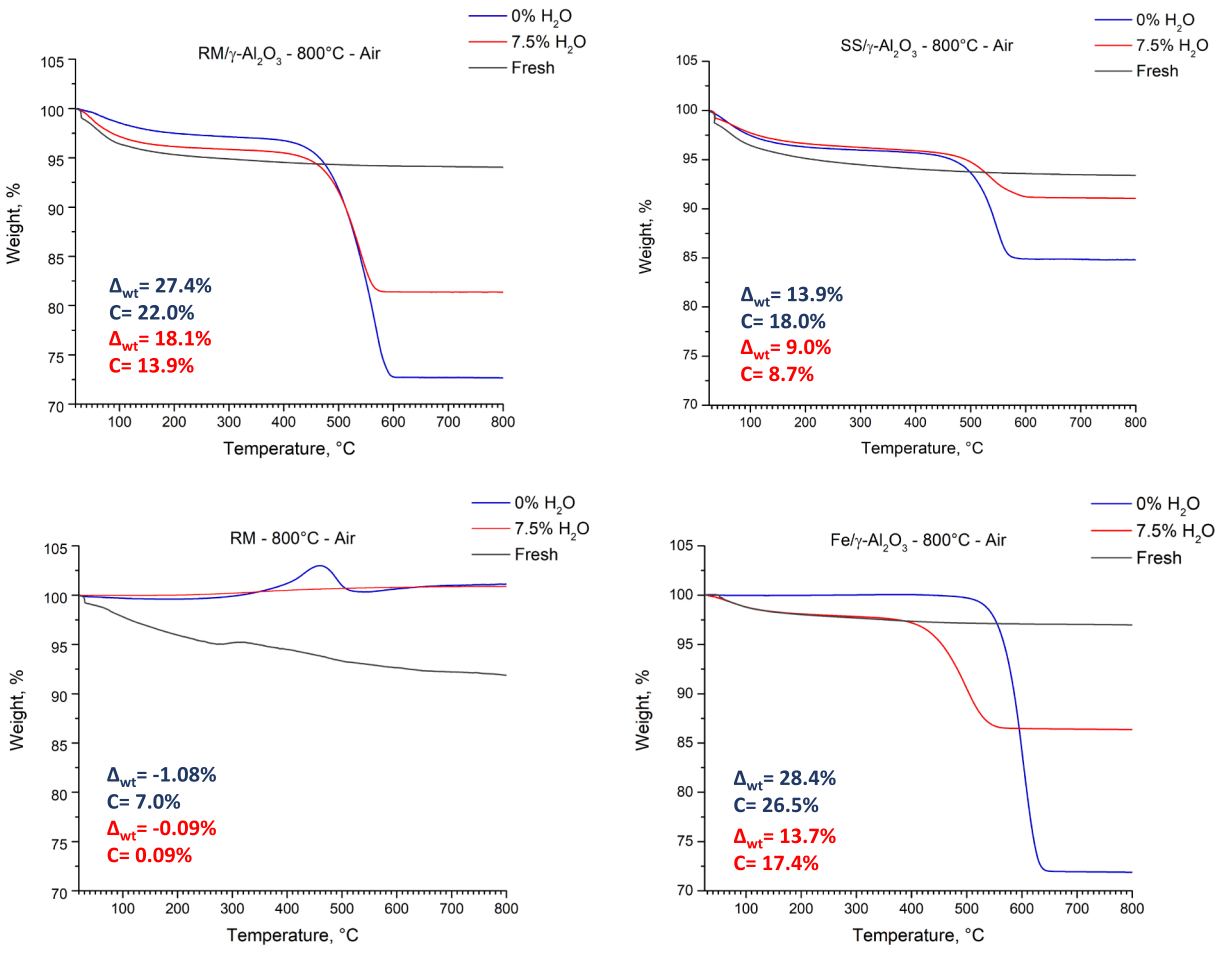

Fig. 8. Thermogravimetric analysis of the different catalysts tested at 800 °C, without and with 7.5 % of steam.

the surface of pure RM, since low carbon concentrations (7 %, without steam, and 0.09 %, with steam) were measured. This indicates that catalyst oxidation caused by air (i.e., the amount of oxygen on the surface) was greater than the amount of carbon deposited by cracking and reforming reactions, resulting in a mass gain.

3.3. Characterisation of the spent catalysts

3.3.1. Porosity measurements

Table 2 shows - for each fresh catalyst and for spent catalyst from tests at 800 °C, with and without steam - the values of specific surface area and volume of pores. Just for spent catalysts, the table also reports data of masked specific surface area, defined as the ratio between the masked surface (obtained as the difference between those of fresh catalyst and spent catalyst) and the surface of the fresh catalyst. No micropores were detected since the catalyst porosity depends on the mesoporous nature of the support used.

RM has the highest surface coverage compared to the others (more than 80 %), under all the operating conditions tested. In the absence of the support, the combined effect of catalyst degradation due to the abrasion of the carrier gases at high temperatures (as confirmed by the negative mass variation reported in Fig. 8), together with a strong tendency to sintering, led to a remarkable loss of active surface. The other supported catalysts show values of masked specific surface almost three times lower than RM, since active metals are bound to the support surface and there is no sintering phenomenon. Without steam, the percentage of masked surface is the highest; with steam, it decreases since part of coke is converted through WG and steam reforming reactions.

Table 2
Porosimetric analysis of the catalysts tested at 800 °C, without and with 7.5 % of steam.

	Catalyst status (Temperature, °C)	Steam concentration, %	Surface area, m^2/g	Pore volume, cm^3/g	Masked specific surface area, %
RM	Fresh (25 °C)	–	95	0.20	–
	Spent (800 °C)	0	16.7	0.07	82
	Spent (800 °C)	7.5	10.6	0.08	89
RM/γ-Al_2O_3	Fresh (25 °C)	–	156	0.45	–
	Spent (800 °C)	0	116.5	0.26	25
	Spent (800 °C)	7.5	121.1	0.32	22
SS/γ-Al_2O_3	Fresh (25 °C)	–	147	0.41	–
	Spent (800 °C)	0	93.5	0.19	36
	Spent (800 °C)	7.5	100.6	0.25	32
Fe/γ-Al_2O_3	Fresh (25 °C)	–	147	0.46	–
	Spent (800 °C)	0	102	0.20	31
	Spent (800 °C)	7.5	129	0.37	12

The values for RM/γ-Al_2O_3 and SS/γ-Al_2O_3 are rather similar to those of Fe/γ-Al_2O_3, even though the latter shows a stronger decrease in masked surface area due to steam action, from 31 % to 12 %, together with the greatest mass variation (0.97 mg/min) among all supported catalysts. This difference could be attributed to the sintering of AAEM elements, such as potassium, at high temperatures (Morris & Bartholomew, 2015), which are not as strongly bound to the surface as in the case of the iron in Fe/γ-Al_2O_3. Sintering causes the increase in the size of the crystallites on the surface which obstruct the pores of the waste-derived catalysts, contributing to the loss of specific surface area. However, any study about mechanism and extension of sintering is complicated by the complex composition of the two waste-derived catalysts.

3.3.2. SEM-EDX analysis

Figs. B.4 and B.5 in ANNEX B report the SEM-EDX analyses of the different spent catalysts, as obtained by tests at 800 °C, without steam (Fig. B.4) and with steam (Fig. B.5). The SEM images on the left side of the two figures indicate that the supported catalysts show rather homogeneous surface, with the presence of different clusters, which could be attributed to several elements deposited on the surface. The images on the middle of the two figures report the mapping of all the elements recognised in a thickness of 2 μm by EDX analysis. It is noteworthy that, in this kind of analyses, the element with the greatest thickness and concentration overlays the others, which are deposited in thinner layers. The mapping of the Fe/γ-Al_2O_3 catalyst shows this behaviour since the presence of the γ-Al_2O_3 support makes it difficult to distinguish the thin layer of iron. Instead, both SS/γ-Al_2O_3 and RM/γ-Al_2O_3 do not show this effect: for SS/γ-Al_2O_3 the main element on the surface is silica under both the operating conditions, while for RM/γ-Al_2O_3 a heterogeneous layer, containing Fe and Mn as main elements, is instead present. Finally, with reference to spent samples of pure RM, that from tests without steam (Fig. B.4), presents Fe and Al as the main elements, with less oxygen compounds compared to that from tests with steam, so confirming the iron reduction operated by H_2. The EDX images reported in the right column of the two figures, refer instead only to the carbon layer, which appears masking all the tested catalysts. Nevertheless, carbon is not present in the overlay images (of the middle), indicating a thickness lower than 2 μm, which is anyway sufficient to partially deactivate the catalyst (Boccia et al., 2021; Parrillo et al., 2023). The carbon maps also show some darker areas representing the metal clusters and indicating a lower deposition rate in that spot. The coke can be distinguished according to the location in where it is deposited (Ochoa et al., 2020), namely: (i) coke deposited on metal particles (also known as encapsulating coke); (ii) coke deposited at the metal-promoter/support interface; (iii) coke deposited on support. While coke (i) is readily accessible by steam and converted more easily, coke (ii) and (iii) may be produced after a longer residence time and are less reactive towards WG and steam reforming reactions. This means that naphthalene, which is bound to the active site during the reaction, is more easily converted to lighter gases and the production of coke (or a thicker layer of it) is not favoured, resulting in a slower deactivation.

4. Conclusions

The catalytic efficiency of two waste-derived materials, red mud (RM/γ-Al_2O_3) and sewage sludge (SS/γ-Al_2O_3), for tar cracking reactions was investigated. The role of the support was studied by testing red mud catalysts with and without the γ-alumina support.

The research quantified the naphthalene conversion efficiencies and time evolution of generated gases during the cracking process in long-term tests, carried out under different values of process temperatures (750 °C-800 °C) and steam concentrations (0 %–7.5 %). The performance of each waste-derived catalyst was compared with that of a pure iron-based catalyst (Fe/γ-Al_2O_3).

The Fe/γ-Al_2O_3 catalyst shows the highest hydrogen yield with steam, confirming the positive activity of iron as steam reforming catalyst. However, the naphthalene conversion efficiencies of all the γ-Al_2O_3 supported catalysts are rather similar throughout the tests and remained almost constant in a range between 60 % and 80 %. This seems to confirm the role of AEEMs, which help to hinder the coke deposition, as it is highlighted by the measured lower mass increasing of the waste-derived catalysts (about 0.20 mg/min, 0.48/min for RM/γ-Al_2O_3, SS/γ-Al_2O_3, respectively) compared with that (0.97 mg/min) of Fe/γ-Al_2O_3. The pure RM shows instead a loss of catalyst mass, highlighting the role of support, which helps to prevent sintering and loss of catalytic elements during the process.

The tests allowed following the evolution of physical and chemical characteristics of the catalysts and characterising the coke layers deposition on the catalyst surfaces. The XRD spectra of RM catalyst show different oxidation states of iron depending on the operating conditions: without steam, it is detected as Fe^0 (the most reduced form), with steam it is detected as magnetite (the intermediate oxidation form). Tuning the steam concentration appears then important to keep constant the reduced state of iron while limiting coke deposition, that is known as the main cause of catalyst deactivation.

Further studies are necessary to better highlight the strengths and weaknesses of these waste-derived materials, by using a real syngas flow, so helping a reliable assessment of the potential for their utilisation as catalysts in hot syngas cleaning. They could be a key element of an efficient strategy to reduce the cost of tar removal in waste gasification processes and, at the same time, provide an alternative for a valuable treatment of these residual wastes.

CRediT authorship contribution statement

Francesco Parrillo: Writing – original draft, Validation, Software, Methodology, Investigation, Funding acquisition, Formal analysis, Data curation, Conceptualization. **Filomena Ardolino:** Software, Investigation, Data curation. **Carmine Boccia:** Writing – original draft, Visualization, Validation, Software, Methodology, Investigation, Formal analysis, Data curation, Conceptualization. **Vincenzo Arconati:** Writing – original draft, Software, Methodology, Investigation, Formal analysis, Data curation. **Giovanna Ruoppolo:** Software, Methodology, Formal analysis, Data curation. **Umberto Arena:** Writing – review & editing, Writing – original draft, Visualization, Validation, Supervision, Project administration, Funding acquisition, Conceptualization.

Declaration of competing interest

The authors declare that they have no known competing financial interests or personal relationships that could have appeared to influence the work reported in this paper.

Data availability

Data will be made available on request.

Acknowledgements

This work was carried out with the financial support of the Project 1.3 “Oxygen and Steam Gasification of Plastics: Process design and techno-scientific support to the executive design of a large-scale pilot plant” founded by The Italian Ministry of Environment and Energy Security in the framework of the Research on Electric System programme, Research Plan 2022-2024; and of the Project GAP (ImprovinG circularity of challenging plastics waste by gAsification Process), founded by the University of Campania “Luigi Vanvitelli” to support fundamental and applied research projects dedicated to young researchers, according to the Strategic Plan 2021-2023 of the University (D.R. n. 509 of 13 June 2022).

The authors gratefully acknowledge the important and continuous support given by Mr. Andrea Capuozzo and Mr. Luigi Stanzione,

technicians of the Institute of Sciences and Technologies for Sustainable Energy and Mobility (STEM) of the Italian National Research Council-CNR.

Appendix A. Supplementary data

Supplementary data to this article can be found online at https://doi.org/10.1016/j.wasman.2024.03.006.

References

Alreshaidan, S.B., Ibrahim, A.A., Fakeeha, A.H., Almutlaq, A.M., Ali, F.A.A., Al-Fatesh, A. S., 2022. Effect of modified alumina support on the performance of ni-based catalysts for CO_2 reforming of methane. Catalysts 12 (9), 1066. https://doi.org/10.3390/catal12091066.

Altomare, A., Corriero, N., Cuocci, C., Falcicchio, A., Moliterni, A., Rizzi, R., 2015. QUALX2.0: a qualitative phase analysis software using the freely available database POW-COD. J. Appl. Cryst. 48 (2), 598–603. https://doi.org/10.1107/S1600576715002319.

Anis, S., Zainal, Z.A., 2011. Tar reduction in biomass producer gas via mechanical, catalytic and thermal methods: a review. Renew. Sustain. Energy Rev. 15, 2355–2377. https://doi.org/10.1016/j.rser.2011.02.018.

Arena U., 2013. Fluidized bed gasification. Chap. 17 in: Fluidized Bed Technologies for Near-Zero Emission Combustion and Gasification. Woodhead Publishing, 765–812. Doi: 10.1533/9780857098801.3.765.

Ashok, J., Dewangan, N., Das, S., Hongmanorom, P., Wai, M.H., Tomishige, K., Kawi, S., 2020. Recent progress in the development of catalysts for steam reforming of biomass tar model reaction. Fuel Process. Technol. 199, 106252 https://doi.org/10.1016/j.fuproc.2019.106252.

Bartholomew C.H., Farrauto R.J., 2010. Fundamentals Of Industrial Catalytic Processes. 2nd ed. John Wiley & Sons. ISBN: 978-0-471-73007-1.

Behrens M., Schlögl R., 2012. X-Ray Diffraction and Small Angle X-Ray Scattering. Chap 15 in: Characterization of Solid Materials and Heterogeneous Catalysts: From Structure to Surface Reactivity. 1st ed., Wiley-VCH Verlag GmbH & Co, 611–653. Doi: 10.1002/9783527645329.ch15.

Bian, Z., Das, S., Wai, M.H., Hongmanorom, P., Kawi, S., 2017. A review on bimetallic nickel-based catalysts for CO_2 reforming of methane. ChemPhysChem 18, 3117–3134. https://doi.org/10.1002/cphc.201700529.

Boccia, C., Parrillo, F., Ruoppolo, G., Commodo, M., Berruti, F., Arena, U., 2021. The effect of steam concentration on hot syngas cleaning by activated carbons. Fuel Process. Technol. 224, 107033 https://doi.org/10.1016/j.fuproc.2021.107033.

Brostow, W., Datashvili, T., 2008. Chemical modification and characterization of boehmite particles. Ch&ChT 2, 1–6.

Busca, G., 2019. Catalytic materials based on silica and alumina: structural features and generation of surface acidity. Prog. Mater Sci. 104, 215–249. https://doi.org/10.1016/j.pmatsci.2019.04.003.

Cheng, L., Wu, Z., Zhang, Z., Guo, C., Ellis, N., Bi, X., Watkinson, A.P., Grace, J.R., 2020. Tar elimination from biomass gasification syngas with bauxite residue derived catalysts and gasification char. Appl. Energy 258, 114088. https://doi.org/10.1016/j.apenergy.2019.114088.

Chi, H., Andolina, C.M., Li, J., Curnan, M.T., Saidi, W.A., Zhou, G., Yang, J.C., Veser, G., 2018. Dependence of H_2 and CO_2 selectivity on cu oxidation state during partial oxidation of methanol on Cu/ZnO. Appl. Catal. A 556, 64–72. https://doi.org/10.1016/j.apcata.2018.02.028.

Chianese, S., Loipersböck, J., Malits, M., Rauch, R., Hofbauer, H., Molino, A., Musmarra, D., 2015. Hydrogen from the high temperature water gas shift reaction with an industrial Fe/Cr catalyst using biomass gasification tar rich synthesis gas. Fuel Process. Technol. 132, 39–48. https://doi.org/10.1016/j.fuproc.2014.12.034.

Dayton, D.C., Turk, B., Gupta, R., 2019. Syngas cleanup, conditioning, and utilization. chap 5 in: thermochemical processing of biomass: conversion into fuels, chemicals and power, 2nd ed. John Wiley & Sons Ltd. https://doi.org/10.1002/9781119417637.ch5.

Das, B., Mohanty, K., 2019. A review on advances in sustainable energy production through various catalytic processes by using catalysts derived from waste red mud. Renew. Energy 143, 1791–1811. https://doi.org/10.1016/j.renene.2019.05.114.

Daza, Y.A., Kuhn, J.N., 2016. CO_2 conversion by reverse water gas shift catalysis: comparison of catalysts, mechanisms and their consequences for CO_2 conversion to liquid fuels. RSC Adv 6, 49675–49691. https://doi.org/10.1039/c6ra05414e.

Di Gregorio, F., Parrillo, F., Salzano, E., Cammarota, F., Arena, U., 2016. Removal of naphthalene by activated carbons from hot gas. Chem. Eng. J. 291, 244–253. https://doi.org/10.1016/j.cej.2016.01.081.

Djandja, O.S., Duan, B., Yin, L.X., Cao, C., Shan, Y., Duo, J., Yao, G., Duan, P.G., 2022. Ammonia-assisted thermal hydrolysis of sewage sludge: solid and liquid phases characterization. Sustainable Energy Technol. Assess. 53, 102693 https://doi.org/10.1016/j.seta.2022.102693.

Duprez, D., 1992. Selective steam reforming of aromatic compounds on metal catalysts. Appl. Catal. A 82, 111–157. https://doi.org/10.1016/0926-860X(92)85001-R.

Feng, D., Zhao, Y., Zhang, Y., Sun, S., Meng, S., Guo, Y., Huang, Y., 2016. Effects of K and Ca on reforming of model tar compounds with pyrolysis biochars under H_2O or CO_2. Chem. Eng. J. 306, 422–432. https://doi.org/10.1016/j.cej.2016.07.065.

Fuentes-Cano, D., Parrillo, F., Ruoppolo, G., Gomez-Barea, A., Arena, U., 2018. The influence of the char internal structure and composition on heterogeneous conversion of naphthalene. Fuel Process. Technol. 172, 125–132. https://doi.org/10.1016/j.fuproc.2017.12.015.

Gao, X., Wang, Z., Ashok, J., Kawi, S., 2020. A comprehensive review of anti-coking, anti-poisoning and anti-sintering catalysts for biomass tar reforming reaction. Chemical Engineering Science: X 7, 100065. https://doi.org/10.1016/j.cesx.2020.100065.

Gou, M., Hou, W., Zhou, L., Zhao, J., Zhao, M., 2023. Preparation and properties of calcium aluminate cement with Bayer red mud. Constr. Build. Mater. 373, 130827 https://doi.org/10.1016/j.conbuildmat.2023.130827.

Guan, G., Kaewpanha, M., Hao, X., Abudula, A., 2016. Catalytic steam reforming of biomass tar: prospects and challenges. Renew. Sustain. Energy Rev. 58, 450–461. https://doi.org/10.1016/j.rser.2015.12.316.

He, L., Hu, S., Jiang, L., Liao, G., Chen, X., Han, H., Xiao, L., Ren, Q., Wang, Y., Su, S., Xiang, J., 2018. Carbon nanotubes formation and its influence on steam reforming of toluene over Ni/Al_2O_3 catalysts: roles of catalyst supports. Fuel Process. Technol. 176, 7–14. https://doi.org/10.1016/j.fuproc.2018.03.007.

Hunston, C., Baudouin, D., Tarik, M., Kröcher, O., Vogel, F., 2021. Investigating active phase loss from supported ruthenium catalysts during supercritical water gasification. Cat. Sci. Technol. 11, 7431–7444. https://doi.org/10.1039/D1CY00379H.

Huygens, D., Garcia-Gutierrez, P., Orveillon, G., Schillaci, C., Delre, A., Orgiazzi, A., Wojda, P., Tonini, D., Egle, L., Jones, A., Pistocchi, A., Lugato, E., 2022. Screening risk assessment of organic pollutants and environmental impacts from sewage sludge management. Publications Office of the European Union, Luxembourg.

Jansen, D., Gazzani, M., Manzolini, G., van Dijk, E., Carbo, M., 2015. Pre-combustion CO_2 capture. Int. J. Greenhouse Gas Control 40, 167–187. https://doi.org/10.1016/j.ijggc.2015.05.028.

Jenness, G.R., Christiansen, M.A., Caratzoulas, S., Vlachos, D.G., Gorte, R.J., 2014. Site-dependent Lewis acidity of γ-Al_2O_3 and its impact on ethanol dehydration and etherification. J. Phys. Chem. C 118, 12899–12907. https://doi.org/10.1021/jp5028349.

Kang, B.S., Farooq, A., Valizadeh, B., Lee, D., Seo, M.W., Jung, S.C., 2023. Valorization of sewage sludge via air/steam gasification using activated carbon and biochar as catalysts. Int. J. Hydrogen Energy. https://doi.org/10.1016/j.ijhydene.2023.04.188.

Kapelari, S., Gamaletsos, P.N., Pilla, G., Pontikes, Y., Blanpain, B., 2023. Developing a low-temperature, carbon-lean hybrid valorisation process for bauxite residue (red mud) towards metallic fe and al recovery. Journal of Sustainable Metallurgy 9, 578–587. https://doi.org/10.1007/s40831-023-00648-7.

Kharaji, A.G., Shariati, A., Takassi, M.A., 2013. A novel γ-alumina supported Fe-Mo bimetallic catalyst for reverse water gas shift reaction. Chin. J. Chem. Eng. 21, 1007–1014. https://doi.org/10.1016/S1004-9541(13)60573-X.

Koike, M., Li, D., Watanabe, H., Nakagawa, Y., Tomishige, K., 2015. Comparative study on steam reforming of model aromatic compounds of biomass tar over ni and ni-fe alloy nanoparticles. Appl. Catal. A 506, 151–162. https://doi.org/10.1016/j.apcata.2015.09.007.

Li, D., Tamura, M., Nakagawa, Y., Tomishige, K., 2015. Metal catalysts for steam reforming of tar derived from the gasification of lignocellulosic biomass. Bioresour. Technol. 178, 53–64. https://doi.org/10.1016/j.biortech.2014.10.010.

Lysenko, E.N., Surzhikov, A.P., Zhuravkov, S.P., Vlasov, V.A., Pustovalov, A.V., Yavorovsky, N.A., 2014. The oxidation kinetics study of ultrafine iron powders by thermogravimetric analysis. Journal Thermal Analysis and Calorimetry 115, 1447–1452. https://doi.org/10.1007/s10973-013-3456-x.

Madadkhani, S., Burhenne, L., Bi, X., Ellis, N., Grace, J.R., Lewis, T., 2021. Bauxite residue as an iron-based catalyst for catalytic cracking of naphthalene, a model compound for gasification tar. Can. J. Chem. Eng. 99, 1461–1474. https://doi.org/10.1002/cjce.23872.

Mahinroosta, M., Karimi, Z., Allahverdi, A., 2020. Recycling of red mud for value-added applications: a comprehensive review. Encyclopedia Renewable Sustainable Mater. Elsevier vol. 1–5, 561–582. https://doi.org/10.1016/B978-0-12-803581-8.11474-2.

Marsh, H., Rodriguez-Reinoso, F., 2006. Activated carbon, 1st ed. 9780080444635, Elsevier ISBN.

Meng, J., Zhao, Z., Wang, X., Chen, J., Zheng, A., Huang, Z., Wei, G., Li, H., 2019. Steam reforming and carbon deposition evaluation of phenol and naphthalene used as tar model compounds over ni and fe olivine-supported catalysts. J. Energy Inst. 92, 1765–1778. https://doi.org/10.1016/j.joei.2018.12.004.

Miccio, F., Picarelli, A., Ruoppolo, G., 2016. Increasing tar and hydrocarbons conversion by catalysis in bubbling fluidized bed gasifiers. Fuel Process. Technol. 141, 31–37. https://doi.org/10.1016/j.fuproc.2015.06.007.

Morris, D.A., Bartholomew, C.H., 2015. Heterogeneous catalyst deactivation and regeneration: a review. Catalysts 5, 145–269. https://doi.org/10.3390/catal5010145.

Mosallanejad, S., Dlugogorski, B.Z., Kennedy, E.M., Stockenhuber, M., 2018. On the chemistry of iron oxide supported on γ-alumina and silica catalysts. ACS Omega 3, 5362–5374. https://doi.org/10.1021/acsomega.8b00201.

Nath, H., Sahoo, P., Sahoo, A., 2015. Characterization of red mud treated under high temperature fluidization. Powder Technol. 269, 233–239. https://doi.org/10.1016/j.powtec.2014.09.011.

Ochoa, A., Arregi, A., Amutio, M., Gayubo, A.G., Olazar, M., Bilbao, J., Castaño, P., 2018. Coking and sintering progress of a ni supported catalyst in the steam reforming of biomass pyrolysis volatiles. Appl. Catal., B 233, 289–300. https://doi.org/10.1016/j.apcatb.2018.04.002.

Ochoa, A., Bilbao, J., Gayubo, A.G., Castaño, P., 2020. Coke formation and deactivation during catalytic reforming of biomass and waste pyrolysis products: a review. Renew. Sustain. Energy Rev. 119, 109600 https://doi.org/10.1016/j.rser.2019.109600.

Parrillo, F., Ruoppolo, G., Arena, U., 2020. The role of activated carbon size in the catalytic cracking of naphthalene. Energy 190, 116385. https://doi.org/10.1016/j.energy.2019.116385.

Parrillo, F., Boccia, C., Ruoppolo, M., Commodo, M., Berruti, F., Arena, U., 2023. Steam reforming of tar in hot syngas cleaning by different catalysts: removal efficiency and coke layer characterization. Can. J. Chem. Eng. 1–13 https://doi.org/10.1002/cjce.24535.

Prins, R., 2020. On the structure of γ-Al_2O_3. J. Catal. 392, 336–346. https://doi.org/10.1016/j.jcat.2020.10.010.

Qi, Y., 2021. The neutralization and recycling of red mud – a review. J. Phys. Conf. Ser. 1759, 012004 https://doi.org/10.1088/1742-6596/1759/1/012004.

Ravenni, G., Sárossy, Z., Sanna, S., Ahrenfeldt, J., Henriksen, U.B., 2020. Residual gasification char applied to tar reforming in a pilot-scale gasifier: performance and evolution of char properties for perspective cascade uses. Fuel Process. Technol. 210, 106456 https://doi.org/10.1016/j.fuproc.2020.106546.

Rostrup-Nielsen, J.R., 1984. Catalytic steam reforming. chap 1 in: Catalysis. 1–117. https://doi.org/10.1007/978-3-642-93247-2_1.

Ruoppolo, G., Miccio, F., Miccio, M., Brachi, P., Chirone, R., 2021. Sewage sludge ashes as a primary catalyst for the abatement of tar in biomass gasification: bubbling versus spouted-fluidized bed configuration. Can. J. Chem. Eng. 99, 1706–1714. https://doi.org/10.1002/cjce.24083.

Shin, S., Kim, M.-J., 2024. Hydrothermal synthesis of zeolites from residual waste generated via indirect carbonation of coal fly ash. Sustainable Environ. Res. 34, 1. https://doi.org/10.1186/s42834-023-00206-6.

Silveira, N.C.G., Martins, M.L.F., Bezerra, A.C.S., Araújo, F.G.S., 2021. Red mud from the aluminium industry: production, characteristics, and alternative applications in construction materials—a review. Sustainability 13. https://doi.org/10.3390/su132212741.

Talebkeikhah, F., Sun, S., Luterbacher, J.S., 2023. Sinter-resistant nickel catalyst for lignin hydrogenolysis achieved by liquid phase atomic layer deposition of alumina. Adv. Energy Mater. 13, 2203377. https://doi.org/10.1002/aenm.202203377.

Umansky, B.S., Hall, W.K., 1990. A spectrophotometric study of the acidity of some solid acids. J. Catal. 124, 97–108. https://doi.org/10.1016/0021-9517(90)90106-T.

Wang, S., Jin, H., Deng, Y., Xiao, Y., 2021. Comprehensive utilization status of red mud in China: A Critical review. J. Clean. Product. 289, 125136. https://doi.org/10.1016/j.jclepro.2020.125136.

Wang, G., Wang, Y., Lv, J., Wu, Y., Jin, L., Li, Y., Yang, H., Hou, B., Hu, H., 2022b. Effect of red mud-based additives on the formation characteristics of tar and gas produced during coal pyrolysis. J. Energy Inst. 104, 1–11. https://doi.org/10.1016/j.joei.2022.06.009.

Wang, J., Zhang, S., Xu, D., Zhang, H., 2022a. Catalytic activity evaluation and deactivation progress of red mud/carbonaceous catalyst for efficient biomass gasification tar cracking. Fuel 323, 124278. https://doi.org/10.1016/j.fuel.2022.124278.

Yeo, T.Y., Ashok, J., Kawi, S., 2019. Recent developments in Sulphur-resilient catalytic systems for syngas production. Renew. Sustain. Energy Rev. 100, 52–70. https://doi.org/10.1016/j.rser.2018.10.016.

Yung, M.M., Jablonski, W.S., Magrini-Bair, K.A., 2009. Review of catalytic conditioning of biomass-derived syngas. Energy Fuel 23, 1874–1887. https://doi.org/10.1021/ef800830n.

Zhang, Q., Bu, T., Lu, J., Jin, Z., Chen, D., Qiu, F., Feng, Y., Hu, W., 2022. Effects of quicklime conditioning on the volatile reforming and tar elimination performance of sewage sludge pyrochar. J. Anal. Appl. Pyrol. 168, 105732 https://doi.org/10.1016/j.jaap.2022.105732.

Zhang, J., Chen, T., Jiao, Y., Wang, L., Wang, J., Chen, Y., Zhu, Q., Li, X., 2020. Role of acidity in catalytic cracking of n-decane over supported Pt-based catalysts. Appl. Surf. Sci. 507, 145113 https://doi.org/10.1016/j.apsusc.2019.145113.

Zhang, Y., Wang, Y., Cui, H., Wang, F., Li, Z., Sun, C., Jia, Y., Xie, Y., Song, F., Wang, J., Yi, W., 2024. Co-pyrolysis of biomass with red mud: an efficient approach to improving bio-oil quality and resourceful utilization of the iron in red mud. Fuel 355, 129482. https://doi.org/10.1016/j.fuel.2023.129482.